Monthly Notices
of the
ROYAL ASTRONOMICAL SOCIETY

MNRAS **433,** 2564–2575 (2013)
Advance Access publication 2013 June 20

doi:10.1093/mnras/stt931

Optical polarimetry of the inner Crab nebula and pulsar

P. Moran,[1⋆] A. Shearer,[1⋆] R. P. Mignani,[2,3,4] A. Słowikowska,[4] A. De Luca,[3,5] C. Gouiffès[6,7] and P. Laurent[6,8]

[1]*Centre for Astronomy, NUI Galway, University Road, Galway, Ireland*
[2]*MSSL UCL, Holmbury St. Mary, Dorking, Surrey RH5 6NT, UK*
[3]*INAF - Istituto di Astrofisica Spaziale e Fisica Cosmica Milano, via E. Bassini 15, I-20133, Milano, Italy*
[4]*Kepler Institute of Astronomy, University of Zielona Góra, Lubuska 2, PL-65-265 Zielona Góra, Poland*
[5]*INFN Istituto Nazionale di Fisica Nucleare, sezione di Pavia, via A. Bassi 6, I-27100 Pavia, Italy*
[6]*CEA, IRFU, Service d'Astrophysique, F-91191 Gif-sur-Yvette, France*
[7]*AIM, CEA/CNRS/Université Paris Diderot, SAp, Saclay, F-91191 Gif-sur-Yvette, France*
[8]*APC, 10 rue Alice Domont et Leonie Duquet, F-75205 Paris Cedex 13, France*

Accepted 2013 May 23. Received 2013 May 23; in original form 2013 February 6

ABSTRACT

Time-resolved polarization measurements of pulsars offer a unique insight into the geometry of their emission regions. Such measurements provide observational constraints on the different models proposed for the pulsar emission mechanisms. Optical polarization data of the Crab nebula were obtained from the *Hubble Space Telescope* (*HST*) archive. The data set consists of a series of observations of the nebula taken with the *HST*/Advanced Camera for Surveys (ACS). We produced polarization vector maps of the inner nebula and measured, for the first time, the degree of linear polarization (P.D.) and the position angle (P.A.) of the pulsar's integrated pulse beam, and of its nearby synchrotron knot. This yielded P.D. $= 5.2 \pm 0.3$ per cent and P.A. $= 105\overset{\circ}{.}1 \pm 1\overset{\circ}{.}6$ for the pulsar, and P.D. $= 59.0 \pm 1.9$ per cent and P.A. $= 124\overset{\circ}{.}7 \pm 1\overset{\circ}{.}0$ for the synchrotron knot. This is the first high-spatial resolution multi-epoch study of the polarization of the inner nebula and pulsar. None of the main features in the nebula shows evidence of significant polarization evolution in the period covered by these observations. The results for the pulsar are consistent with those obtained by Słowikowska et al. using the high-time resolution photo-polarimeter – Optical Pulsar Timing Analyzer (OPTIMA), once the constant component (DC) component has been subtracted. Our results clearly prove that the knot is the main source of the DC component.

Key words: polarization – radiation mechanisms: non-thermal – stars: neutron – pulsars: general – pulsars: individual: the Crab pulsar.

1 INTRODUCTION

Strong polarization is expected when the pulsar optical emission is generated by synchrotron radiation. Shklovsky (1953) suggested that the continuous optical radiation from the Crab nebula was due to synchrotron radiation. This was later confirmed by Dombrovsky (1954) and Vashakidze (1954) who found that the optical radiation was polarized. Incoherent synchrotron emission follows a simple relationship between its polarization profile and underlying geometry. Hence, optical polarization measurements of pulsars provide a unique insight into the geometry of their emission regions, and therefore observational constraints on the theoretical models of the emission mechanisms. From an understanding of the emission geometry, one can limit the competing models for pulsar emission, and hence understand how pulsars work – a problem which has eluded astronomers for almost 50 years.

⋆E-mail: p.moran4@nuigalway.ie (PM); andy.shearer@nuigalway.ie (AS)

Polarimeters are sensitive in the optical, but the majority of pulsars are very faint at these wavelengths with $V \geq 25$ (Shearer 2008). Polarimetry in the very high-energy domain, X-ray and gamma-ray, using instruments on board space telescopes, is of limited sensitivity. So far, detailed results have only been reported for the Crab pulsar (Weisskopf et al. 1978; Dean et al. 2008; Forot et al. 2008). Although the number of pulsars detected in the optical is growing, only five pulsars have had their optical polarization measured: Crab (Wampler, Scargle & Miller 1969; Kristian et al. 1970; Smith et al. 1988; Słowikowska et al. 2009), Vela (Wagner & Seifert 2000; Mignani et al. 2007), PSR B0540−69 (Middleditch, Pennypacker & Burns 1987; Chanan & Helfand 1990; Wagner & Seifert 2000; Mignani et al. 2010) PSR B0656+14 (Kern et al. 2003) and PSR B1509−58 (Wagner & Seifert 2000). Nonetheless, the optical currently remains invaluable for polarimetry in the energy domain above radio photon energies. The Crab pulsar, being the brightest optical pulsar with $V \approx 16.8$ (Nasuti et al. 1996), has had several measurements of its optical

polarization, including both phase-averaged and phase-resolved studies.

The first phase-resolved observations of the optical linear polarization of the Crab pulsar were those of Wampler et al. (1969), Cocke et al. (1970) and Kristian et al. (1970). Those studies showed that the polarization position angle (P.A.) changes through each peak in the pulsar light curve, and that the degree of polarization falls and rises within each peak, reaching its minimum value shortly after the pulse peak. These observations were limited to the main and inter pulse phase regions only, because at the time it was thought that the pulsar radiated its optical emission through the pulse peaks only. However, a number of phase-resolved imaging observations of the pulsar (Peterson et al. 1978; Jones, Smith & Wallace 1981; Percival et al. 1993; Golden et al. 2000) showed that the optical emission actually persists throughout the pulsar's entire rotation cycle, at the level of ∼1 per cent of the maximum main-pulse intensity.

With this in mind, observations of the optical linear polarization of the Crab pulsar were made by Jones et al. (1981) and Smith et al. (1988). These results confirmed the previous observations, and were the first studies to reveal the polarization profile of the pulsar during the bridge and off-pulse phase regions. They also found that the off-pulse region is highly polarized. The degree of polarization was 70 per cent and 47 ± 10 per cent for Jones et al. (1981) and Smith et al. (1988), respectively. Słowikowska et al. (2009) report the most detailed phase-resolved observations of the optical linear polarization of the Crab pulsar. Their results are consistent with previous observations albeit with better definition and statistics, and can be explained in the context of the two-pole caustic model (Dyks, Harding & Rudak 2004), the outer-gap model (Romani & Yadigaroglu 1995; Takata 2007) and the striped-wind model (Pétri & Kirk 2005).

Detailed observations of the inner nebula, in the optical and X-rays, have revealed a torus structure, that is bisected by oppositely directed jets, knots and a series of highly variable synchrotron wisps (Scargle 1969; Hester et al. 1995; Weisskopf et al. 2000). A bright knot of synchrotron emission is located 0.65 arcsec SE of the pulsar. It is highly polarized and is slightly variable in both its location and its brightness (Hester et al. 1995, 2002; Hester 2008). Komissarov & Lyutikov (2011) proposed that it is radiation from an oblique termination shock in the pulsar wind nebula. In this model, the Earth line of sight is tangent to the flow at the position of the knot, hence the intensity is Doppler boosted for synchrotron emission in the mildly relativistic post-shock flow. The results of their relativistic magnetohydrodynamic (MHD) simulations show that the knot is highly variable and can dominate the gamma-ray synchrotron emission. It has been suggested that this knot is responsible for the highly polarized off-pulse emission seen in time-resolved observations in the optical (Słowikowska et al. 2009, 2013) and gamma-rays (Forot et al. 2008). The knot has no counterpart to the NW of the pulsar, but there is a faint second knot located 3.8 arcsec SE of the pulsar, the so-called outer knot.

The wisps consist of Wisp 1, a Thin wisp located 1.8 arcsec NW of the pulsar, and the Counter wisp located 8.3 arcsec SE of the pulsar. Wisp 1, located 7.3 arcsec NW of the pulsar, breaks into three separate and distinct components: 1-A, 1-B and 1-C (Scargle 1969). However, one must note that this does not represent the constant configuration of the wisps. The wisps are interpreted as magnetic flux tubes that undergo unstable synchrotron cooling (Hester 1998). A number of follow-up observations of the inner nebula have confirmed the presence of the wisps (Hester et al. 1995; Bietenholz et al. 2004). The NW wisps are more prominent than the SE wisps due to Doppler beaming of the flow. Schweizer et al. (2013) studied the behaviour of the wisps NW of the pulsar in both the optical and X-rays. They observed that the wisps form and move off from the region associated with the termination shock of the pulsar wind, roughly once per year. Moreover, they found that the precise locations of the NW wisps in the optical and X-rays are similar but not exactly coincident, with X-ray wisps located closer to the pulsar. This would suggest that the optical and X-ray wisps are not produced by the same particle distribution. In terms of MHD models, they found that the optical wisps are more strongly Doppler-boosted than the X-ray wisps. For a more detailed review of the Crab nebula see Hester (2008).

The first optical linear polarization maps of the Crab nebula were produced by Oort & Walraven (1956), Hiltner (1957) and Woltjer (1957). X-ray observations of the linear polarization of the nebula, in the range 2.6–5.2 keV, yield polarization of 19 per cent at a P.A. of 152–156° within a radius of 3° of the pulsar (Weisskopf et al. 1978). These results are in agreement with the optical measurements of the polarization, which give polarization of 19 per cent at a P.A. 162° for the central nebular region within a radius of ≈0.5 arcmin (Oort & Walraven 1956). Dean et al. (2008) measured the polarization of the Crab nebula and pulsar in the off-pulse phase using the International Gamma-ray Astrophysics Laboratory/Spectrometer on *INTEGRAL* (*INTEGRAL*/SPI) telescope, and showed that the polarization E-vector (124 ± 11°) is aligned with the spin-axis of the neutron star (Kaplan et al. 2008; 110 ± 2 ± 9°, where the first uncertainty is the measurement uncertainty and the second is from the reference frame uncertainty). This result was later confirmed by Forot et al. (2008), in the off-pulse phase region using the *INTEGRAL*/Imager on-Board the *INTEGRAL* Satellite (IBIS) telescope (120.°6 ± 8.°5), and has also been seen in optical observations (Smith et al. 1988; Słowikowska et al. 2009). The SPI and IBIS measurements both encompass the entire nebula and pulsar, and so are dominated by nebular emission. As with the optical observations (Smith et al. 1988; Słowikowska et al. 2009), they found the off-pulse region to be highly polarized.

The purpose of this work is two fold. First, we want to check the polarization of the pulsar, knot and wisps for variability. It is difficult to determine the polarization for objects embedded in a strong nebular background. So, in order to determine the Crab pulsar's polarization profile, we need to know the level of background polarization. Therefore, the second purpose of this work is to accurately map the polarization of the inner Crab nebula. This will then act as a guideline for future time-resolved polarization measurements of the Crab pulsar using the Galway Astronomical Stokes Polarimeter (GASP). This is an ultra-high-speed, full Stokes, astronomical imaging polarimeter based on the Division of Amplitude Polarimeter (DOAP). It has been designed to resolve extremely rapid variations in objects such as optical pulsars and magnetic cataclysmic variables (Kyne et al. 2010).

2 OBSERVATIONS AND ANALYSIS

The raw *Hubble Space Telescope*/Advanced Camera for Surveys (*HST*/ACS) polarization science frames of the Crab nebula were obtained from the Mikulski Archive for Space Telescopes (MAST). The data set consists of 13 observations of the nebula taken in three different polarisers (0°, 60°and 120°) between 2003 August and 2005 December (Proposal ID: 9787) (see Table 1). The Wide Field Camera (WFC) detector, called ACS/WFC, employs a mosaic of two 4096 × 2048 Scientific Imaging Technologies (SITe) CCDs, with a pixel-scale of ∼0.05 arcsec pixel^{-1}, covering a nominal field of view (FOV) ∼202 × 202 arcsec^2 (Pavlovsky et al. 2004).

Table 1. Summary of the *HST*/ACS observations of the Crab nebula. The filters used were *F606W* ($\lambda = 590.70$ nm, $\Delta\lambda = 250.00$ nm) and *F550M* ($\lambda = 558.15$ nm, $\Delta\lambda = 54.70$ nm).

Date	Exposure (s)	Filter	Polarizer	Roll-angle (PA_V3) (°)	Pulsar position on chip (x,y)
2003 Aug 08	2 × 1200	*F606W*	POL0V	87.6	1320.30 1045.02
	2 × 1200		POL60V		
	2 × 1200		POL120V		
2005 Sept 06	2 × 1150	*F550M*	CLEAR2L	87.2	1316.23 1034.54
	2 × 1150	*F606W*	POL0V		
	2 × 1150		POL60V		
	2 × 1150		POL120V		
2005 Sept 15	2 × 1150	*F550M*	CLEAR2L	87.4	1315.58 1042.01
	2 × 1150	*F606W*	POL0V		
	2 × 1150		POL60V		
	2 × 1150		POL120V		
2005 Sept 25	2 × 1150	*F550M*	CLEAR2L	87.6	1315.92 1041.17
	2 × 1150	*F606W*	POL0V		
	2 × 1150		POL60V		
	2 × 1150		POL120V		
2005 Oct 02	2 × 1150	*F550M*	CLEAR2L	87.8	1315.97 1040.11
	2 × 1150	*F606W*	POL0V		
	2 × 1150		POL60V		
	2 × 1150		POL120V		
2005 Oct 12	2 × 975	*F550M*	CLEAR2L	88.0	1316.44 1039.62
	2 × 975	*F606W*	POL0V		
	2 × 1000		POL60V		
	2 × 1000		POL120V		
2005 Oct 22	2 × 1150	*F550M*	CLEAR2L	88.3	1316.66 1038.13
	2 × 1150	*F606W*	POL0V		
	2 × 1150		POL60V		
	2 × 1150		POL120V		
2005 Oct 30	2 × 1150	*F550M*	CLEAR2L	88.6	1316.40 1036.31
	2 × 1150	*F606W*	POL0V		
	2 × 1150		POL60V		
	2 × 1150		POL120V		
2005 Nov 08	2 × 1150	*F550M*	CLEAR2L	89.0	1316.23 1034.54
	2 × 1140	*F606W*	POL0V		
	2 × 1150		POL60V		
	2 × 1150		POL120V		
2005 Nov 16	2 × 1150	*F550M*	CLEAR2L	89.6	1316.57 1031.40
	2 × 1150	*F606W*	POL0V		
	2 × 1150		POL60V		
	2 × 1150		POL120V		
2005 Nov 25	2 × 1150	*F550M*	CLEAR2L	90.6	1315.74 1025.14
	2 × 1150	*F606W*	POL0V		
	2 × 1150		POL60V		
	2 × 1150		POL120V		
2005 Dec 05	2 × 1150	*F550M*	CLEAR2L	120.0	1279.52 871.13
	2 × 1150	*F606W*	POL0V		
	2 × 1150		POL60V		
	2 × 1150		POL120V		
2005 Dec 14	2 × 1150	F550M	CLEAR2L	125.0	1267.44 851.24
	2 × 1150	*F606W*	POL0V		
	2 × 1150		POL60V		
	2 × 1150		POL120V		

For these observations, with the polarisers in place, the FOV was $\approx$102 × 102 arcsec^2. The filter used was *F606W* ($\lambda = 590.70$ nm, $\Delta\lambda = 250.00$ nm). The raw images, which had already been flat-fielded, were geometrically aligned, combined and averaged with cosmic ray removal using IRAF (see Fig. 1). We used a total of five field stars and the IRAF task CCMAP and the *2MASS* catalogue to fit the astrometry. The pulsar was found at $\alpha = 05^{\rm h}34^{\rm m}31\overset{\rm s}{.}930 \pm 0\overset{\rm s}{.}001$, $\delta = +22^\circ00'51\overset{''}{.}990 \pm 0\overset{''}{.}110$, whilst the synchrotron knot, located 0.65 arcsec SE of the pulsar (Hester et al. 1995) is found at $\alpha = 05^{\rm h}34^{\rm m}31\overset{\rm s}{.}980 \pm 0\overset{\rm s}{.}001$, $\delta = +22^\circ00'51\overset{''}{.}630 \pm 0\overset{''}{.}110$ (the errors denote the rms of the astrometric fit). For each set of observations, the images taken in the different polarisers were analysed

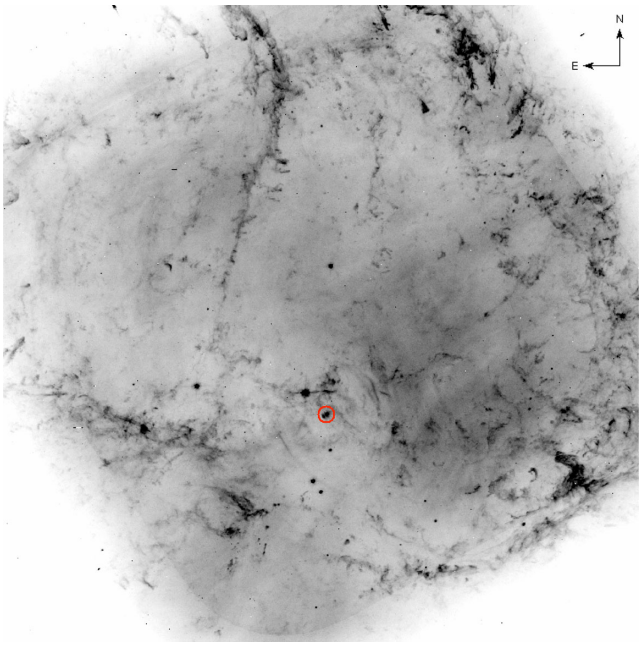

Figure 1. *HST*/ACS image of the inner Crab nebula (2005 Sept 06, FOV ≈ 102 × 102 arcsec^2, *F606W*, POL0V). The location of the pulsar and inner knot is marked by the circle.

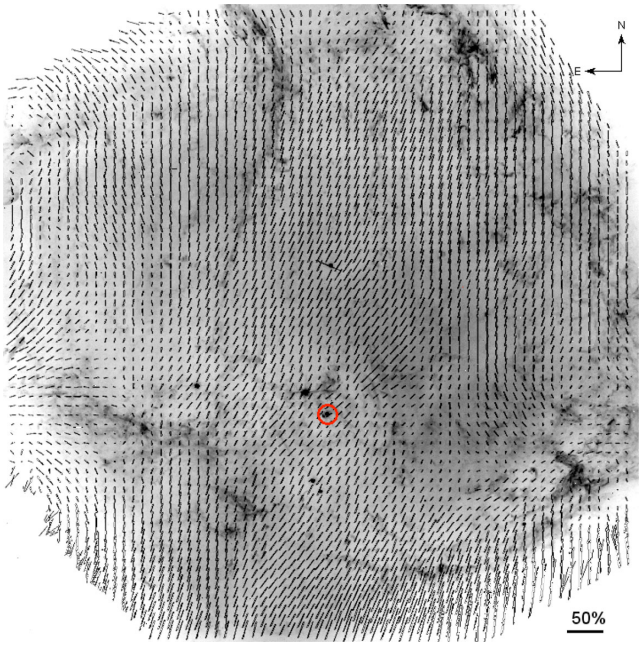

Figure 2. Polarization vector map of the inner Crab nebula superimposed on the nebula (2005 Sept 06, FOV ≈ 102 × 102 arcsec^2). The location of the pulsar and inner knot is marked by the circle. The legend shows the vector magnitude for 50 per cent polarization.

by the IMPOL[1] software (Walsh 1999), which produces polarization maps (see Figs 2 and 3).

In order to determine the polarimetry, aperture photometry was first performed on the pulsar and synchrotron knot in each image using the IRAF task PHOT. The pulsar is saturated in each frame per

[1] http://www.stecf.org/software/IRAFtools/stecf-iraf/impol

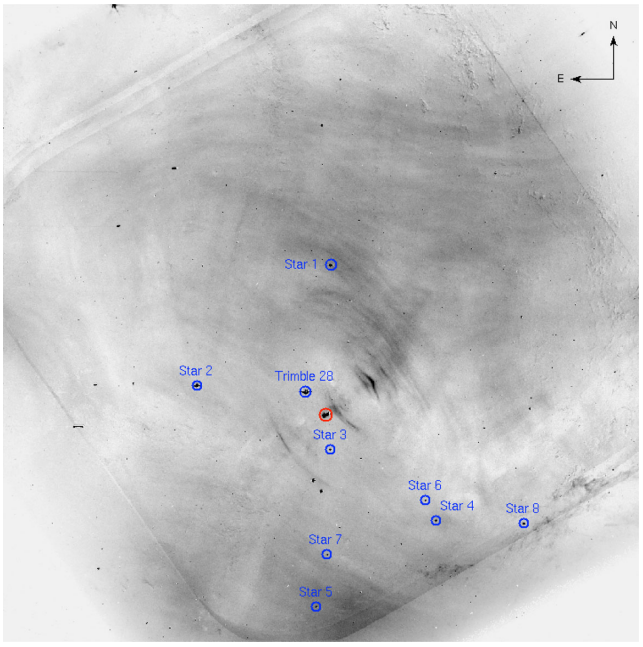

Figure 3. Polarized flux map of the inner Crab nebula (2005 Sept 06, FOV ≈ 102 × 102 arcsec^2) with the stars for analysis marked. The location of the pulsar and inner knot is marked by the circle.

epoch. Gilliland (2004) describes the well-behaved response of the ACS, and shows that electrons are conserved after saturation. The response of the ACS CCDs remains linear up to and beyond the point of saturation provided one uses a gain value that samples the full well depth. For ACS this is a gain equal to 2 e^{-1}/ADU, which is the gain setting used for these observations. Over a range of almost 4 magnitudes, photometry remains linear to <1 per cent. One can perform aperture photometry of isolated point sources by summing over all the pixels that were bled into (Pavlovsky et al. 2004). We tested this method by performing aperture photometry on the pulsar and Trimble 28. We used images taken at the same epoch as the polarimetric observations (2005 September to December) in the *F550M* filter ($\lambda = 558.15$ nm, $\Delta\lambda = 54.70$ nm) but with no polarizer in place. We computed the visual magnitudes of both targets and found that the values are consistent with those of Sandberg & Sollerman (2009), once the different pass bands are taken into account.

We used an aperture of radius 0.25 arcsec to measure the flux from the pulsar. The sky counts were measured using an annulus of width ≈0.1 arcsec, located 0.15 arcsec beyond the central aperture. We added to this flux the flux from the pixels that were bled into. An aperture of radius 0.15 arcsec was used to measure the flux from the synchrotron knot. The sky counts were measured in a region close to the pulsar and knot.

The Stokes parameters were then calculated using the following formulae:

$$I = \frac{2}{3}\,[r(0) + r(60) + r(120)] \quad (1)$$

$$Q = \frac{2}{3}\,[2r(0) - r(60) - r(120)] \quad (2)$$

$$U = \frac{2}{\sqrt{3}}\,[r(60) - r(120)] \quad (3)$$

where $r\,(0)$, $r\,(60)$ and $r\,(120)$ are the calibrated count rates in the 0, 60 and 120° polarized images, respectively (Pavlovsky et al. 2004).

2.1 Computing the degree of linear polarization of a target

The degree of linear polarization (P.D.) is calculated using the Stokes parameters, and factors which correct for cross-polarization leakage in the polarizing filters. This correction is useful for the POLUV filters; values for the parallel and perpendicular transmission coefficients ($T_{\rm par}$ and $T_{\rm perp}$) can be found in fig. 5.4 of the ACS Instrument Handbook (Pavlovsky et al. 2004). These corrections together with the calibration of the source count rates removes the instrumental polarization of the WFC (∼2 per cent) (see equation 4).

2.2 Computing the polarization position angle on the sky of the polarization E-vector

The P.A. is calculated using the Stokes parameters, the roll angle of the *HST* spacecraft (PA_V3 in the data header files) and χ, which contains information about the camera geometry that is derived from the design specifications; for the WFC $\chi = -38.^{\circ}2$ (see equation 5).

$$\text{P.D.} = \frac{\sqrt{Q^2+U^2}}{I}\,\frac{T_{\rm par}+T_{\rm perp}}{T_{\rm par}-T_{\rm perp}} \times 100 \tag{4}$$

$$\text{P.A.} = \frac{1}{2}\tan^{-1}\left(\frac{U}{Q}\right) + \text{PA\_V3} + \chi. \tag{5}$$

An important property of polarization that needs to be considered during analysis is that of bias. This is due to instrumental errors which tend to increase the observed polarization of a target from its true polarization. The effect is negligible when $\eta = \text{p} \times \text{S/N}$ is high (>10), where p is the fractional polarization of the target, and S/N is the signal-to-noise ratio per image. See for example fig. 4 of Sparks & Axon (1999). Since the targets are in the high η regime, the debiasing correction is small and therefore we omit it. We note that for stars 3 and 4, which have low η values, there will be a systematic overestimate of the polarization [see Simmons & Stewart (1984) and Sparks & Axon (1999)]. However, as these have a polarization consistent with zero no further analysis was performed on them to remove bias.

Naghizadeh-Khouei & Clarke (1993) investigated the statistical behaviour of the P.A. of linear polarization using both numerical integrations and data simulations. They found that the distribution of the angle is essentially Gaussian for $\eta > 6$. Hence, we used the formulae of Serkowski (1958, 1962) for our error analysis. We propagated the errors in the count rates to obtain errors for the Stokes parameters *I*, *Q* and *U*. Finally, the errors in the Stokes parameters were propagated through the equations for the errors in the degree of polarization (equation 6) and P.A. (equation 7). As negative polarization is impossible, we used asymmetric error bars for stars 3 and 4. Below are the formulae used for calculating the errors in the degree of polarization and P.A.:

$$\frac{\sigma_{\rm P.D.}}{\text{P.D.}} = \sqrt{\frac{Q^2\sigma_Q^2 + U^2\sigma_U^2}{Q^2+U^2} + \left(\frac{\sigma_I}{I}\right)^2} \tag{6}$$

$$\sigma_{\rm P.A.} = 28.^{\circ}65\,\frac{\sigma_{\rm P.D.}}{\text{P.D.}} \tag{7}$$

where $\sigma_{\rm I}$, $\sigma_{\rm Q}$ and $\sigma_{\rm U}$ are the errors in Stokes parameters I, Q and U, respectively. These errors take into account those introduced by instrumentation and systematics.

The polarization of the synchrotron wisps was also studied (see Tables 2 and 3). To measure the total flux of each wisp, we summed the flux from a series of apertures ($r \approx 0.3$ arcsec) placed along the extent of each wisp. We adopt the standard nomenclature as discussed by Scargle (1969), who noted their temporal variability and strong polarization (see Fig. 4). We have accounted for their temporal motion in our analysis. For the sky background subtraction we use the same region of the nebula as used for the knot. Since the contribution of zodiacal and scattered light to the background is low, we therefore ignore the effect of the background polarization in our analysis.

As a guide to our analysis, a number of fore/background stars in the nebula (see Fig. 3) were also analysed to confirm the methodology which we used, and to cross-check for any systematics. Stars 3 and 4 are not saturated in each frame per epoch, but stars 1, 2 and Trimble 28 are saturated. Therefore we employed the same photometric method as used for the pulsar. We used an aperture of radius 0.35 arcsec to measure the flux from each star. The sky counts were measured using an annulus of width ≈0.1 arcsec, located 0.15 arcsec beyond the central aperture. We have found that all of the stars are consistent, within the errors, with unpolarized sources.

We have omitted the results of the analysis of the 2003 August data set. The sky background is highly variable in one of the raw images. This then causes errors when one calculates the polarization of the wisps and plots the polarization maps for this epoch. We also note that for the 2005 December data set that the roll-angle of the spacecraft was significantly different to other observations. For this data set the diffraction spike from the pulsar crosses the knot. Furthermore, we note that for the 14th December data set the full Moon was 9° away from the pulsar. This might have introduced spurious background levels which would have impacted upon the polarization of the faint extended sources such as the wisps.

Table 2. P.D. (per cent) of the Crab pulsar, synchrotron knot and wisps as a function of time. Wisp 1-A is unresolved from 2005 Sept 06 to 2005 Oct 12 inclusive.

Date	Crab	Knot	Wisp 1-A	Wisp 1-B	Wisp 1-C	Thin Wisp	Counter Wisp
2005 Sept 06	4.9 ± 1.0	59.4 ± 7.3		41.7 ± 3.8	32.1 ± 4.5	36.1 ± 4.0	31.0 ± 4.3
2005 Sept 15	5.0 ± 1.0	60.0 ± 7.0		45.0 ± 4.0	34.5 ± 4.6	37.5 ± 4.4	35.6 ± 4.6
2005 Sept 25	5.4 ± 1.0	62.1 ± 7.1		44.2 ± 4.3	40.7 ± 4.7	38.5 ± 4.7	40.1 ± 5.1
2005 Oct 02	4.9 ± 1.0	62.4 ± 6.9		41.3 ± 4.5	39.7 ± 4.7	37.2 ± 4.5	39.2 ± 5.1
2005 Oct 12	4.6 ± 1.0	60.3 ± 6.6		43.4 ± 4.5	36.8 ± 4.8	32.6 ± 4.7	37.5 ± 5.2
2005 Oct 22	4.3 ± 1.0	61.1 ± 6.6	43.6 ± 4.7	46.2 ± 4.5	37.5 ± 5.0	36.9 ± 4.7	45.1 ± 5.4
2005 Oct 30	4.9 ± 1.0	61.4 ± 6.4	44.1 ± 4.6	44.9 ± 4.6	35.2 ± 4.8	34.8 ± 4.9	42.7 ± 5.6
2005 Nov 08	5.1 ± 1.0	60.9 ± 6.2	41.6 ± 4.3	45.6 ± 4.5	39.3 ± 4.6	35.0 ± 5.0	41.0 ± 5.6
2005 Nov 16	5.6 ± 1.0	59.9 ± 6.4	41.5 ± 4.4	46.0 ± 4.8	42.4 ± 4.7	38.1 ± 5.3	47.9 ± 6.3
2005 Nov 25	5.8 ± 1.0	59.9 ± 6.9	41.4 ± 4.4	40.1 ± 4.8	38.9 ± 4.5	38.6 ± 5.5	41.7 ± 5.9
2005 Dec 05	5.9 ± 1.0	42.8 ± 6.2	32.1 ± 3.7	40.9 ± 4.3	38.9 ± 4.5	38.1 ± 4.7	43.2 ± 5.1
2005 Dec 14	5.1 ± 1.0	43.9 ± 6.6	21.2 ± 3.7	25.2 ± 3.7	40.5 ± 4.5	35.4 ± 5.1	39.1 ± 5.5

Table 3. Polarization P.A.s (°) of the Crab pulsar, synchrotron knot and wisps as a function of time. Wisp 1-A is unresolved from 2005 Sep 06 to 2005 Oct 12 inclusive.

Date	Crab	Knot	Wisp 1-A	Wisp 1-B	Wisp 1-C	Thin Wisp	Counter Wisp
2005 Sept 06	103.5 ± 5.9	123.9 ± 3.5		124.8 ± 2.6	129.1 ± 4.0	128.0 ± 3.1	131.5 ± 3.9
2005 Sept 15	103.2 ± 5.9	124.7 ± 3.4		123.7 ± 2.5	124.7 ± 3.8	125.4 ± 3.3	128.1 ± 3.7
2005 Sept 25	106.6 ± 5.4	125.0 ± 3.3		125.7 ± 2.8	125.6 ± 3.3	125.7 ± 3.5	128.6 ± 3.7
2005 Oct 02	103.5 ± 5.8	125.1 ± 3.2		126.5 ± 3.1	125.6 ± 3.4	126.3 ± 3.5	128.6 ± 3.7
2005 Oct 12	102.6 ± 6.4	124.9 ± 3.2		129.5 ± 3.0	129.8 ± 3.7	127.7 ± 4.2	131.0 ± 3.9
2005 Oct 22	109.7 ± 6.7	125.7 ± 3.1	124.8 ± 3.1	127.2 ± 2.8	125.5 ± 3.8	124.2 ± 3.6	126.7 ± 3.5
2005 Oct 30	104.6 ± 5.8	125.7 ± 3.0	125.0 ± 3.0	130.3 ± 3.0	127.8 ± 3.9	126.8 ± 4.0	129.6 ± 3.8
2005 Nov 08	106.6 ± 5.7	125.4 ± 2.9	123.4 ± 3.0	130.6 ± 2.8	129.3 ± 3.3	127.1 ± 4.1	130.7 ± 3.9
2005 Nov 16	108.0 ± 5.1	124.7 ± 3.1	124.5 ± 3.0	130.0 ± 3.0	129.6 ± 3.2	128.0 ± 4.0	131.5 ± 3.8
2005 Nov 25	102.2 ± 5.1	125.4 ± 3.3	125.5 ± 3.0	127.4 ± 3.5	130.2 ± 3.3	125.9 ± 4.1	129.5 ± 4.1
2005 Dec 05	107.5 ± 4.9	121.6 ± 4.2	122.0 ± 3.3	125.7 ± 3.0	130.5 ± 3.2	124.4 ± 3.5	127.3 ± 4.4
2005 Dec 14	102.5 ± 5.7	119.9 ± 4.3	132.6 ± 5.1	131.4 ± 4.2	134.4 ± 3.1	139.2 ± 4.2	143.2 ± 4.0

Table 4. P.D. (per cent) of Trimble 28 and the background stars as a function of time.

Date	Trimble 28	Star 1	Star 2	Star 3	Star 4
2005 Sept 06	1.0 ± 0.7	1.5 ± 1.3	0.9 ± 0.9	$1.6^{+2.8}_{-1.6}$	$3.4^{+3.7}_{-3.4}$
2005 Sept 15	1.1 ± 0.6	2.4 ± 1.3	1.2 ± 0.9	$2.6^{+2.8}_{-2.6}$	$3.4^{+3.7}_{-3.4}$
2005 Sept 25	1.7 ± 0.7	2.4 ± 1.4	1.0 ± 0.9	$2.7^{+2.8}_{-2.7}$	$3.3^{+3.7}_{-3.3}$
2005 Oct 02	1.1 ± 0.6	3.1 ± 1.3	1.2 ± 0.9	$1.7^{+2.8}_{-1.7}$	$2.8^{+3.6}_{-2.8}$
2005 Oct 12	0.9 ± 0.7	2.0 ± 1.3	0.9 ± 0.9	$2.0^{+2.8}_{-2.0}$	$2.2^{+3.7}_{-2.2}$
2005 Oct 22	2.1 ± 0.7	2.5 ± 1.3	1.5 ± 0.9	2.9 ± 2.8	4.3 ± 3.7
2005 Oct 30	0.7 ± 0.6	1.5 ± 1.3	1.4 ± 0.9	$2.0^{+2.8}_{-2.0}$	$2.7^{+3.7}_{-2.7}$
2005 Nov 08	1.2 ± 0.7	2.3 ± 1.4	$0.7^{+0.9}_{-0.7}$	3.3 ± 2.8	3.7 ± 3.7
2005 Nov 16	1.6 ± 0.7	$1.2^{+1.3}_{-1.2}$	1.6 ± 0.9	$2.1^{+2.8}_{-2.1}$	$1.8^{+3.7}_{-1.8}$
2005 Nov 25	1.5 ± 0.7	2.0 ± 1.4	1.5 ± 0.9	$2.5^{+2.9}_{-2.5}$	$3.5^{+3.8}_{-3.5}$
2005 Dec 05	1.8 ± 0.7	2.2 ± 1.4	1.2 ± 0.9	$2.2^{+2.9}_{-2.2}$	$3.0^{+3.8}_{-3.0}$
2005 Dec 14	1.9 ± 0.7	2.5 ± 1.4	1.5 ± 0.9	$1.3^{+2.9}_{-1.3}$	$1.5^{+3.7}_{-1.5}$

We have investigated the effects of photometric losses due to charge transfer efficiency (CTE) in the CCDs of the WFC. The effect reduces the apparent brightness of sources, and it requires a photometric correction to restore the measured integrated counts to their 'true' value. The ACS team claims that there is no evidence of photometric losses due to CTE for WFC data taken after 2004. Nonetheless, we applied the correction for CTE (see equation 8) to our photometry and found that it does not change the results of the polarimetry. Below is the formula for the correction for CTE loss. This value is then added to the measured flux.

$$\mathrm{YCTE} = 10^{A} \times \mathrm{Sky}^{B} \times \mathrm{Flux}^{C} \times \frac{Y}{2048} \times \frac{(\mathrm{MJD} - 52333)}{365}, \quad (8)$$

where MJD is the modified Julian date of the observation, and reflects the linear degradation of the CCD with time. The parameters A, B and C are found in table 6.1 of the ACS Instrument Handbook (Pavlovsky et al. 2004).

In order to determine the performance of the ACS as a polarimeter, the ACS team have modelled the complete instrumental effects and the calibration together. This is done so as to quantify the impacts of the remaining uncalibrated systematic errors. They claim that the fractional polarizations will be uncertain at the one-part-in-ten level (e.g. a 20 per cent polarization has an uncertainty of 2 per cent) for strongly polarized targets; and at about the 1 per cent level for weakly polarized targets. The P.A.s will have an uncertainty of about 3°. This is in addition to uncertainties which arise from photon statistics (Pavlovsky et al. 2004). They then checked this calibration against polarized standard stars (5 per cent polarized) and found it to be reliable within the quoted errors (Cracraft & Sparks 2007).

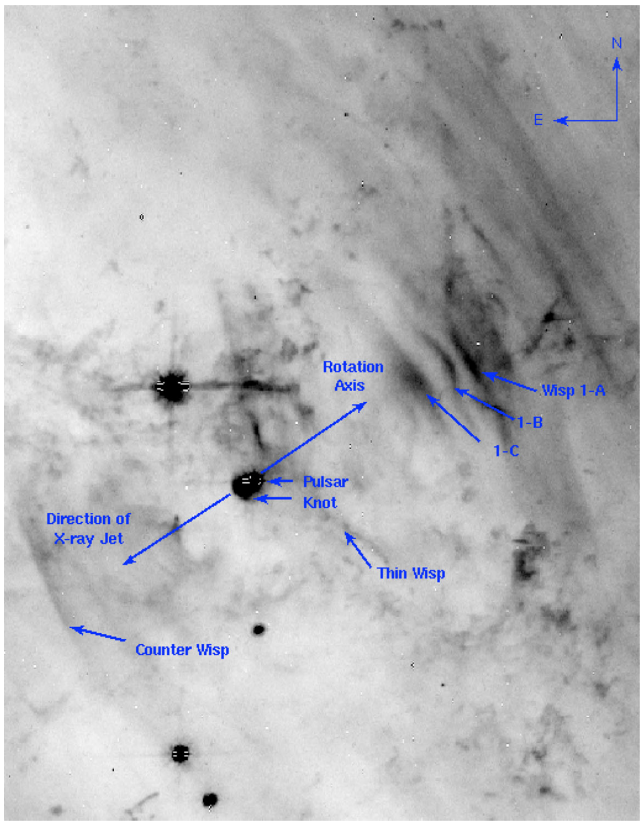

Figure 4. *HST*/ACS image of the vicinity of the Crab pulsar (2005 Nov 25, FOV ≈ 25 × 33 arcsec^2), with features labelled for discussion.

2.3 Photometry and morphology of the knot in unpolarized light

We also retrieved from the MAST archive a series of 12 ACS/WFC data sets, collected through the *F550M* filter ($\lambda = 558.15$ nm, $\Delta\lambda = 54.70$ nm) at the same epoch as the polarimetric observations (from 2005 September 6 to 2005 December 14). Each observation consists of a sequence of two images collected in a single orbit, to

Table 5. Polarization P.A. (°) of Trimble 28 and the background stars as a function of time.

Date	Trimble 28	Star 1	Star 2	Star 3	Star 4
2005 Sept 06	116.3 ± 18.5	149.5 ± 25.8	177.0 ± 28.1	139.3 ± 49.5	146.6 ± 30.7
2005 Sept 15	170.8 ± 17.6	145.3 ± 15.9	174.4 ± 22.2	138.7 ± 31.4	136.2 ± 30.7
2005 Sept 25	159.4 ± 11.1	148.2 ± 12.6	124.2 ± 25.2	145.7 ± 30.5	144.4 ± 32.0
2005 Oct 02	178.5 ± 16.3	151.1 ± 19.4	1.0 ± 20.5	125.9 ± 47.0	148.1 ± 36.9
2005 Oct 12	74.8 ± 20.5	151.1 ± 18.6	97.6 ± 27.1	148.9 ± 39.7	145.8 ± 47.1
2005 Oct 22	152.4 ± 8.0	147.4 ± 15.4	138.8 ± 17.1	148.8 ± 28.3	148.6 ± 24.5
2005 Oct 30	140.0 ± 24.9	153.8 ± 26.3	136.7 ± 17.9	150.8 ± 41.0	142.2 ± 38.3
2005 Nov 08	155.6 ± 15.1	151.3 ± 16.5	124.2 ± 36.8	149.0 ± 24.5	139.5 ± 29.0
2005 Nov 16	156.8 ± 12.0	144.5 ± 33.2	116.3 ± 15.7	140.2 ± 38.7	144.4 ± 60.1
2005 Nov 25	142.6 ± 12.2	153.8 ± 19.9	136.6 ± 17.0	135.3 ± 33.0	149.6 ± 30.9
2005 Dec 05	135.5 ± 10.4	132.4 ± 17.3	144.2 ± 22.2	146.4 ± 37.4	146.1 ± 36.2
2005 Dec 14	144.1 ± 10.1	148.7 ± 15.8	164.9 ± 17.0	150.4 ± 64.5	149.1 ± 69.2

allow for cosmic ray rejection. We retrieved pipeline-calibrated, *drizzled*[2] images from the archive. Total exposure times range from 1950 s to 2300 s per epoch (see Table 1). We superimposed the images on the first-epoch one by using the coordinates of 30 non-saturated field sources as a reference grid. The rms accuracy was better than 0.07 pixels per coordinate. We performed multi-epoch photometry of the knot with the SExtractor software (Bertin & Arnouts 1996). We used an implementation of the Kron method (Kron 1980), which measures the flux of an object within an optimized elliptical aperture, evaluated using the second moments of the object's brightness distribution. The parameters of the Kron ellipse (centre, semiaxes and orientation) also yield a measure of the object coordinates and morphology, which is useful for the case of the knot, which is possibly variable in both position and shape as a function of time. The measured count rate was converted to flux using the standard ACS photometric calibration tabulated in the image headers. Correction for CTE losses proved to have a negligible effect.

Since the knot is a diffuse source located very close to a much brighter and saturated point source (the Crab pulsar), particular care was devoted to estimate systematic errors possibly affecting the flux measurements. To this aim, we have performed simulations with the ESO/Midas software,[3] adding to the ACS images a 'synthetic knot'. A two-dimensional Gaussian function was used to generate the artificial source, setting one of the symmetry axes aligned to the pulsar spin-axis. The synthetic knot was positioned to the NW of the pulsar, along the direction of the pulsar spin-axis, at an angular distance comparable to that of the true knot. By varying the flux and the position of the artificial source we evaluated the uncertainty on the flux measurement to be ∼2.5 per cent.

We also measured the fluxes of a sample of non-saturated stars in the field as a further assessment of the stability of photometry in the variable background of the Crab nebula (see Fig. 3).

3 RESULTS

Included here are the measurements of the degree of polarization and P.A. of each target per epoch (see Tables 2–5 inclusive). We have plotted the degree of polarization and P.A. for each target as a function of time (see Figs 5 and 6). Using a χ^2 goodness-of-fit, we found no significant variation (at the 95 per cent confidence level) in the polarization of the pulsar, knot and wisps over the 3 month period of these observations. As a final comparison, we present the mean values. These are the values obtained from using the weighted mean and error of the degree of polarization and P.A. (see Table 6). Stars 3 and 4 have asymmetric error bars. Hence, we use the method of Barlow (2004) for calculating the weighted mean for asymmetric error bars. As can be seen from Figs 5 and 6 and Table 6, the 2005 December data set shows evidence of a possible variation of the knot polarization at the 2σ level. This variation is due neither to a known systematic effect nor to the contribution of the diffraction spikes from the pulsar (see Section 2.2), which only affect the knot's flux by $\lesssim$2 per cent. Future polarimetry observations on a longer time-span will help us to address the possible knot variability. Similarly, we note that the polarization of Wisps 1-A and 1-B also shows a possible variation at the 2σ level in the 2005 December data set. As discussed in Section 2.2, this may be partially ascribed to the enhanced Moon contribution to the background. This possible variation may be also ascribed to the unresolved contribution of the bright torus in the nebula, to which Wisps 1-A and B have moved closest in the 2005 December observations.

The polarization maps (Figs 2 and 7) show the variation of the polarization throughout the inner nebula and particularly in the vicinity of the pulsar itself. Each vector has magnitude equal to the degree of polarization, and its orientation is the P.A. at that point. Such maps allow one to visualize the direction of the magnetic field lines within the nebula. One can distinctly see the overall structure of the inner nebula, the degree of polarization of the knots and the synchrotron emission. In particular, the filaments are unpolarized and the structures that are visible in polarized light (Fig. 3) do not map exactly the continuum (Fig. 1).

The *F550M* band images were used to study with high accuracy possible displacements of the knot. The light curve of the knot is shown in Fig. 8, compared to the one of the reference stars. The knot is seen to brighten by ∼40 per cent on a 60-d time-scale, then to fade to its initial flux level. Reference stars, conversely, do not display any significant variability. Focusing on the knot, we note that changes in flux are accompanied by shifts in position, the knot centroid being closer to the pulsar when the feature is brighter (the displacement between maximum and minimum flux is 0.075 ± 0.025 arcsec). There is no statistically significant evidence of a change in the full width at half-maximum of the knot as a function of time. We checked our photometric results by repeating

[2] Single, calibrated ACS images were combined using the multidrizzle software, which also produces a mosaic image of the two ACS chips and applies a correction for the geometric distortions of the camera.
[3] http://www.eso.org/sci/software/esomidas/

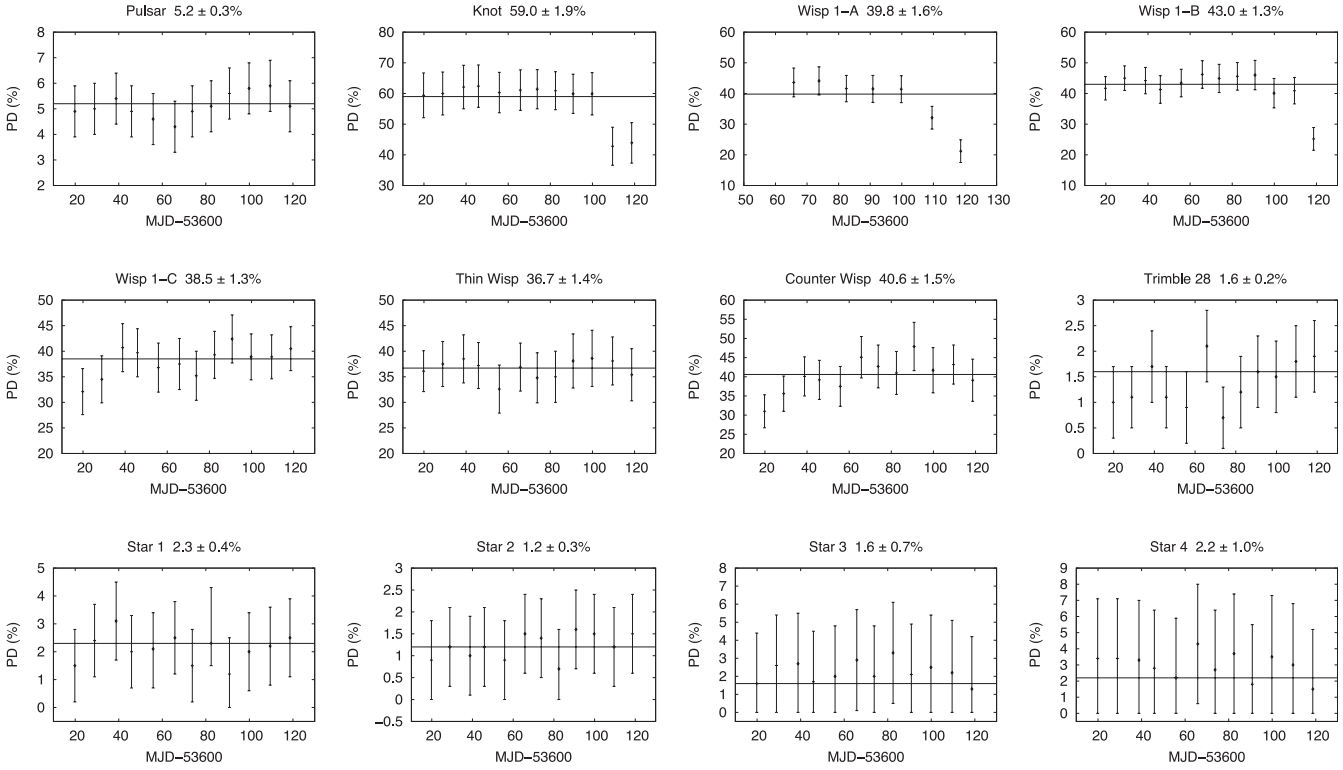

Figure 5. Plots of the P.D. (per cent) of the sources as a function of time. The solid lines are the weighted mean of the degree of polarization.

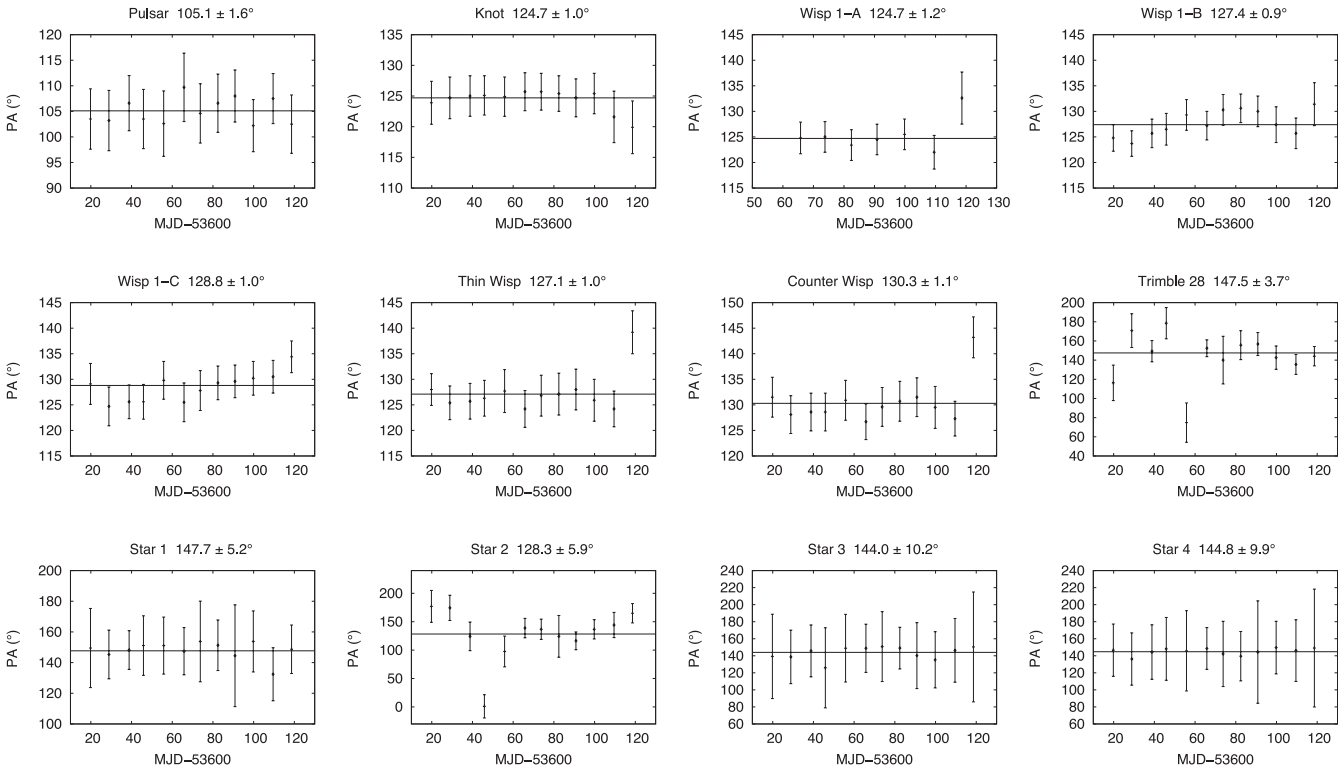

Figure 6. Plots of the polarization P.A. (°) of the sources as a function of time. The solid lines are the weighted mean of the P.A.

Table 6. Overall results for the P.D. (per cent) and P.A. (°). These are the weighted mean and error of the degree of polarization and P.A.

	Polarization degree (per cent)	Position angle (°)
Pulsar	5.2 ± 0.3	105.1 ± 1.6
Synchrotron knot	59.0 ± 1.9	124.7 ± 1.0
Wisp 1-A	39.8 ± 1.6	124.7 ± 1.2
Wisp 1-B	43.0 ± 1.3	127.4 ± 0.9
Wisp 1-C	38.5 ± 1.3	128.8 ± 1.0
Thin Wisp	36.7 ± 1.4	127.1 ± 1.0
Counter Wisp	40.6 ± 1.5	130.3 ± 1.1
Trimble 28	1.6 ± 0.2	147.5 ± 3.7
Star 1	2.3 ± 0.4	147.7 ± 5.2
Star 2	1.2 ± 0.3	128.3 ± 5.9
Star 3	1.6 ± 0.7	144.0 ± 10.2
Star 4	2.2 ± 1.0	144.8 ± 9.9

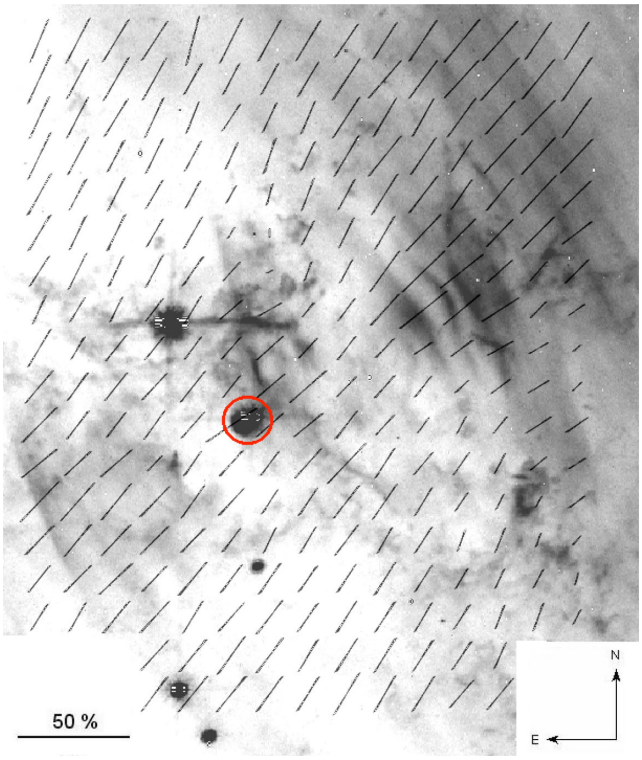

Figure 7. Polarization vector map of the vicinity of the Crab pulsar superimposed on the nebula (2005 Nov. 25, FOV ≈25 × 33 arcsec^2). The location of the pulsar and inner knot is marked by the circle. The legend shows the vector magnitude for 50 per cent polarization.

the analysis with simple aperture photometry, using an aperture of 0.15 arcsec positioned on the knot centroid (as measured in each epoch). Such an exercise yielded consistent results (∼40 per cent brightening in two months), confirming the significant variability in flux.

4 DISCUSSION

We have studied the phase-averaged polarization properties of the Crab pulsar and its nearby synchrotron knot using archival *HST*/ACS data. We note that the data set analysed in this paper has previously been used by Hester (2008) to examine the morphology and structure of the polarized components of the inner nebula. However, we have produced polarization vector maps of the inner

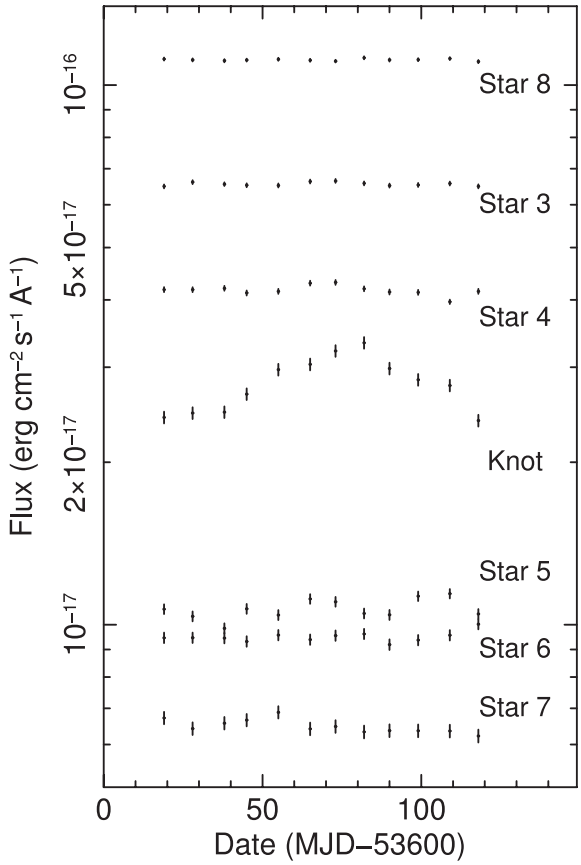

Figure 8. Results of photometry on the knot as well as on a sample of field stars. A large flux variability for the knot is apparent, with a ∼40 per cent brightening on a two-month time-scale.

nebula and measured, for the first time, the P.D. and the P.A. of the pulsar's integrated pulse beam, and of its nearby synchrotron knot. Furthermore, this work marks the first high-spatial resolution multi-epoch study of the variability of the polarization of the inner nebula and pulsar.

The results for the Crab pulsar are P.D. = 5.2 ± 0.3 per cent, and P.A. = 105.°1 ± 1.°6 (see Table 6). These values are in good agreement with those of Słowikowska et al. (2009) using the high time resolution photo-polarimeter – Optical Pulsar Timing Analyzer (OPTIMA)[4] (Kanbach et al. 2008), once the constant component (DC) is subtracted. They measure phase-averaged values of P.D. = 9.8 ± 0.1 per cent, and P.A. = 109.°5 ± 0.°2, which is not DC subtracted and includes the emission from the inner knot due to the OPTIMA aperture. They measure values of P.D. = 5.4 per cent, and P.A. = 96.°4 after DC subtraction, and it is this latter measurement that agrees with our own. The optical polarization of the Crab pulsar has also been measured by Wampler et al. (1969) (P.D. = 6.5 ± 0.9 per cent, P.A. = 107.°0 ± 6.°0), and Kristian et al. (1970) (P.D. = 6.8 ± 0.5 per cent, P.A. = 98.°0 ± 3.°0).

We note that the polarization of the inner knot (59.0 ± 1.9 per cent) is a factor of 2 larger than the off-pulse polarization of 33 per cent obtained from OPTIMA observations (Słowikowska et al. 2009) and consistent with the older measurements of Jones et al. (1981) (70 per cent) and Smith et al. (1988) (47 ± 10 per cent). This discrepancy is partially due to the uncertainty of determining

[4] http://www.mpe.mpg.de/OPTIMA

the phase interval bracketing the minimum of the Crab's light curve, hence the contribution of the DC component (see fig. 5 of Słowikowska et al. 2009). It could also be partially due to uncertainties in the estimate of the sky background in the OPTIMA data and/or the contribution from the sky and pulsar 'off-pulse' flux. Golden et al. (2000) give the unpulsed pulsar flux to be 0.02 mJy compared to 0.03 mJy from the knot (this work). We estimate the contribution from the sky for OPTIMA data to be equivalent to 0.04 mJy based on the pupil size of 2.35 arcsec and a 21 magnitude arcsec^{-2} sky background. This would be sufficient to explain the difference. Two-dimensional phase-resolved polarization observations will allow us to better quantify the knot contribution to the DC component.

X-ray observations of the nebula taken by *Chandra* (Weisskopf et al. 2000) reveal a torus with bipolar jets emanating outwards from SE and NW of the pulsar. Ng & Romani (2006) found that the axis of symmetry of the jet is roughly aligned with the pulsar's proper motion vector. The Crab torus, bisecting the synchrotron wisps, can be traced back to the knot of synchrotron emission seen ≈0.65 arcsec SE of the pulsar. Our measurement of the polarization P.A. of the synchrotron knot, P.A. = 124.°7 ± 1.°0, agrees with the Crab torus P.A. = 126.°31 ± 0.°03 (Ng & Romani 2004). We also found evidence for an apparent alignment between the pulsar polarization P.A. (105.°1 ± 1.°6) and proper motion vector (Kaplan et al. 2008; 110 ± 2 ± 9°) (see Fig. 9). Mignani et al. (2007) have found the same scenario for the Vela pulsar. Those authors found an apparent alignment between the polarization P.A. of the pulsar, the axis of symmetry of the X-ray arcs and jets (*Chandra*; Pavlov et al. 2001; Helfand, Gotthelf & Halpern 2001), and the pulsars proper motion vector. This suggests that the 'kick' given to neutron stars at birth is directed along the rotation axis (Lai, Chernoff & Cordes 2001). The alternative view is that the apparent alignment is an effect of projection on to the sky plane, and that there is no physical jet along the axis of rotation (Radhakrishnan & Deshpande 2001). More concrete measurements of the optical polarization of pulsars will yield the needed observational restraints on these hypotheses.

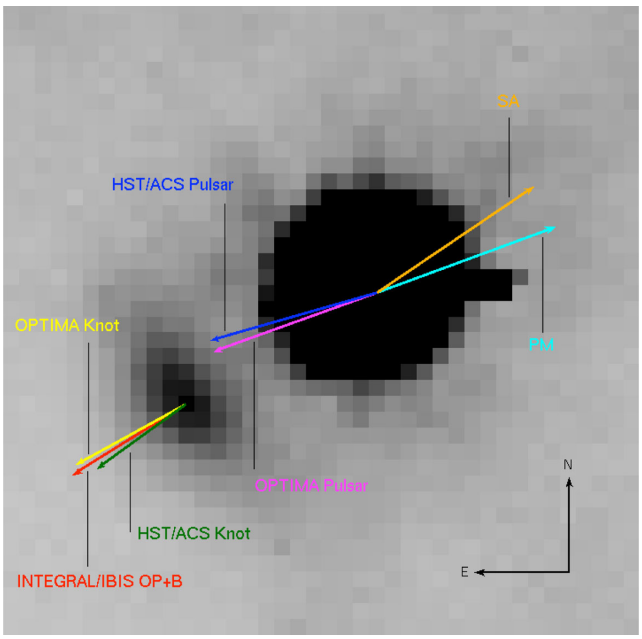

Figure 9. The pulsar region with the synchrotron knot located ≈0.65 arcsec SE of the pulsar (2005 Sept. 06, FOV ≈2 × 2 arcsec^2). The vectors included are as follows: spin-axis vector (SA) (124 ± 0.°1) (Ng & Romani 2004), proper motion vector (PM) (110 ± 2 ± 9°) (Kaplan et al. 2008), and the polarization P.A. of the pulsar (105.°1 ± 1.°6) and synchrotron knot (124.°7 ± 1.°0) from the *HST*/ACS data. Also included are the phase-averaged OPTIMA measurements of the polarization P.A. of the synchrotron knot (119.°8 ± 0.°8) and pulsar (109.°5 ± 0.°2) (Słowikowska et al. 2009), and the phase-averaged *INTEGRAL*/IBIS measurement of the polarization P.A. during the off-pulse and bridge emission (OP+B) phases (122.°0 ± 7.°7) (Forot et al. 2008).

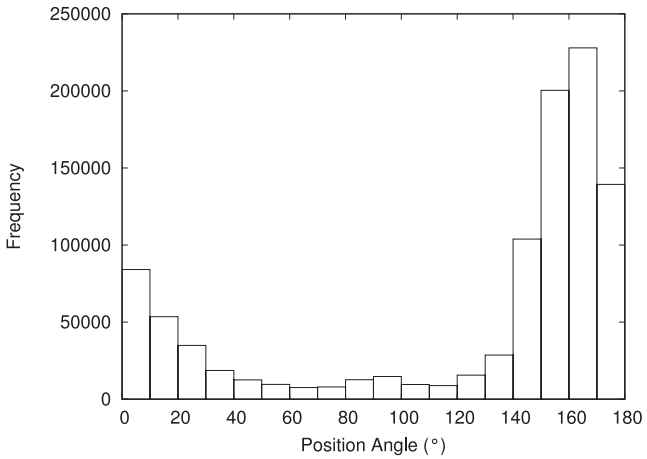

Figure 10. Histogram of the polarization P.A. of the entire inner nebula.

As mentioned previously, the polarization of the wisps was also studied. Our photometry accounts for the outward motion of the wisps. From the analysis of the wisps in each epoch, we find that the wisps show variation in both location and brightness on timescales of a few weeks. We found that all of these wisps have similar values of degree of polarization (∼40 per cent) and P.A. equal to that of the synchrotron knot (∼125°). Hence, as with the synchrotron knot, they are aligned with the spin-axis of the pulsar. Also, Wisps 1-A is not visible in the frames from 2005 September to 2005 October 12 inclusive, and may be merged with Wisp 1-B during this period. Examining the polarization vectors maps, one can see that the P.A. of the wisps are different to those of the rest of the nebula, where the P.A. are aligned NS (Figs 2 and 7). Fig. 10 is a histogram of the distribution of the polarization P.A. of the inner nebula. The P.A. were extracted from the values in the polarization map. From this histogram we see that the polarization P.A. of the pulsar environment (∼125°) is away from the peak of the nebula distribution (∼165°). This means that the polarization properties of the structures close to the pulsar are different from those of the rest of the inner nebula.

As discussed earlier, using a χ^2 goodness of fit, we found no significant variation (at the 95 per cent confidence level) in the polarization of the pulsar, knot and wisps over a 3 month period. The knot is variable in flux but fairly constant in polarization. This variation in flux may be explained in terms of an increased plasma density in the vicinity of the knot. Whereas the wisps have constant flux and constant polarization over this period of time. This would suggest that the magnetic fields within the nebula are uniform over time. However, more detailed follow-up observations will be needed to determine if there is any longer term variation.

5 CONCLUSIONS

We have studied the phase-averaged polarization properties of the Crab pulsar and its nearby synchrotron knot using archival

HST/ACS data. This marks the first high-spatial resolution multi-epoch study of the polarization of the inner nebula and pulsar. We found an apparent alignment between the polarization P.A. of the pulsar and the pulsar's proper motion vector. We confirm that the inner knot is responsible for the highly polarized off-pulse emission seen in observations in the optical. We found that the inner knot is variable in position, and brightness over the period of these observations. These are the first quantified measurements of such a variation. We note that we found evidence of a possible variation of the knot polarization (at 2σ) which is due neither to a known systematic effect nor to the spike contribution. Future observations will help to address this point. We have also measured the polarization of the wisps in the inner nebula, and found no significant variation in their polarization over this 3 month period of observations.

Polarization measurements give a unique insight into the geometry of the pulsar emission regions. More multi-wavelength polarization observations of pulsars, both phase-averaged and phase-resolved, with instruments such as *HST*/ACS and GASP (optical), and *INTEGRAL*/IBIS (gamma-ray), will help to provide the much needed data to constrain the theoretical models.

For example, McDonald et al. (2011) have developed an inverse mapping approach for determining the emission height of the optical photons from pulsars. It uses the optical Stokes parameters to determine the most likely geometry for emission, including: magnetic field inclination angle (α), the observers line-of-sight angle (χ) and emission height.

ACKNOWLEDGEMENTS

All of the data presented in this paper were obtained from the MAST. STScI is operated by the Association of Universities for Research in Astronomy, Inc., under NASA contract NAS5-26555. Support for MAST for non-*HST* data is provided by the NASA Office of Space Science via grant NNX09AF08G and by other grants and contracts. We thank Jeremy Walsh, ESO, for the use of his polarimetry software IMPOL to produce the polarization maps. PM is grateful for his funding from the Irish Research Council (IRC). RPM thanks the European Commission Seventh Framework Programme (FP7/2007-2013) for their support under grant agreement n.267251. ASł acknowledges support from the Foundation for Polish Science grant FNP HOM/2009/11B, as well as from the FP7 Marie Curie European Reintegration Grant (PERG05-GA-2009-249168). This work was in part supported under the FP7 Opticon European Network for High Time Resolution Astrophysics (HTRA) project. We are grateful to the anonymous referee whose comments improved the quality of the final version of the paper.

REFERENCES

Barlow R., 2004, preprint (arXiv:physics/0401042)
Bertin E., Arnouts S., 1996, A&AS, 317, 393
Bietenholz M. F., Hester J. J., Frail D. A., Bartel N., 2004, ApJ, 615, 794
Chanan G. A., Helfand D. J., 1990, ApJ, 352, 167
Cocke W. J., Disney M. J., Muncaster G. W., Gehrels T., 1970, Nat, 227, 1327
Cracraft M., Sparks W. B., 2007, ACS Polarization Calibration – Data, Throughput, and Multidrizzle Weighting Schemes, Tech. rep.
Dean J. et al., 2008, Sci, 321, 1183
Dombrovsky V. A., 1954, Doklady Akad Nauk, USSR, 94, 1021
Dyks J., Harding A. K., Rudak B., 2004, ApJ, 606, 1125
Forot M., Laurent P., Grenier I. A., Gouiffès C., Lebrun F., 2008, ApJ, 688, L29
Gilliland R. L., 2004, Instrument Science Report ACS 04-01
Golden A., Shearer A., Redfern R. M., Beskin G. M., Neizvestny S. I., Neustroev V. V., Plokhotnichenko V. L., Cullum M., 2000, A&A, 363, 617
Helfand D. J., Gotthelf E. V., Halpern J. P., 2001, ApJ, 556, 380
Hester J. J., 1998, in Shibazaki N., ed., Neutron Stars and Pulsars: Thirty Years after the Discovery. Universal Academy Press, Tokyo, p. 431
Hester J. J., 2008, ARA&A, 46, 127
Hester J. J. et al., 1995, ApJ, 448, 240
Hester J. J. et al., 2002, ApJ, 577, L49
Hiltner W. A., 1957, ApJ, 125, 300
Jones D. H. P., Smith F. G., Wallace P. T., 1981, MNRAS, 196, 943
Kanbach G., Stefanescu A., Duscha S., Mühlegger M., Schrey F., Steinle H., Slowikowska A., Spruit H., 2008, in Phelan D., Ryan O., Shearer A., eds, ASSL, Vol. 351, High Time Resolution Astrophysics. Springer, Berlin, p. 153
Kaplan D. L., Chatterjee S., Gaensler B. M., Anderson J., 2008, ApJ, 677, 1201
Kern B., Martin C., Mazin B., Halpern J. P., 2003, ApJ, 597, 1049
Komissarov S. S., Lyutikov M., 2011, MNRAS, 414, 2017
Kristian J., Visvanathan N., Westphal J. A., Snellen G. H., 1970, ApJ, 162, 475
Kron R. G., 1980, ApJS, 43, 305
Kyne G., Sheehan B., Collins P., Redfern M., Shearer A., 2010, in Garcia-Caurel E., de Martino A., eds, API'09 – First NanoCharM Workshop on Advanced Polarimetric Instrumentation, Palaiseau, France, EPJ Web of Conferences, Volume 5, id.05003
Lai D., Chernoff D. F., Cordes J. M., 2001, ApJ, 549, 1111
McDonald J., O Connor P., de Búrca D., Golden A., Shearer A., 2011, MNRAS, 417, 730
Middleditch J., Pennypacker C. R., Burns M. S., 1987, ApJ, 315, 142
Mignani R. P., Bagnulo S., Dyks J., Lo Curto G., Słowikowska A., 2007, A&A, 467, 1157
Mignani R. P., Sartori A., De Luca A., Rudak B., Słowikowska A., Kanbach G., Caraveo P. A., 2010, A&A, 515, A110
Naghizadeh-Khouei J., Clarke D., 1993, A&A, 274, 968
Nasuti F. P., Mignani R., Caraveo P. A., Bignami G. F., 1996, A&A, 314, 849
Ng C.-Y., Romani R. W., 2004, ApJ, 601, 479
Ng C.-Y., Romani R. W., 2006, ApJ, 644, 445
Oort J. H., Walraven T., 1956, Bull. Astron. Inst. Netherlands, 12, 285
Pavlov G. G., Kargaltsev O. Y., Sanwal D., Garmine G. P., 2001, ApJ, 554, L189
Pavlovsky C., Riess A., Mack J., Gilliland R., 2004, in Karakla D., Rose S., eds, ACS Data Handbook, Version 3.0, STScI, Baltimore
Percival J. W. et al., 1993, ApJ, 407, 276
Peterson B. A., Murdin P. G., Wallace P. T., Manchester R. N., Penny A. J., Jorden A. R., Hartley K. F., King D. J, 1978, Nat, 276, 475
Pétri J., Kirk J. G., 2005, ApJ, 627, L37
Radhakrishnan V., Deshpande A. A., 2001, A&A, 379, 551
Romani R. W., Yadigaroglu I. A., 1995, ApJ, 438, 314
Sandberg A., Sollerman J., 2009, A&A, 504, 525
Scargle J. D., 1969, ApJ, 156, 401
Schweizer T., Bucciantini N., Idec W., Nilsson K., Tennant A., Weisskopf M. C., Zanin R., 2013, preprint (arXiv:1301.1321)
Serkowski K., 1958, Acta Astron., 8, 135
Serkowski K., 1962, in Kopal Z., ed., Advances in Astronomy and Astrophysics. Academic Press, p. 289
Shearer A., 2008, in Phelan D., Ryan O., Shearer A., eds, Astrophysics and Space Science Library, Vol. 351, Astrophysics and Space Science Library, High Time Resolution Astrophysics and Pulsars, p. 1
Shklovsky I. S., 1953, Doklady Akad Nauk, USSR, 90, 983
Simmons J. F. L., Stewart B. G., 1984, A&A, 142, 100
Słowikowska A., Kanbach G., Kramer M., Stefanescu A., 2009, MNRAS, 397, 103
Słowikowska A., Mignani R., Kanbach G., Krzeszowski K., 2013, in Lewandowski W., Maron O., Kijak J., eds, ASP Conf. Ser. Vol. 466, Astronomical Society of the Pacific Conference Series. Decomposition

of the Optical Polarization Components of the Crab Pulsar and its Nebula, Astron. Soc. Pac., San Francisco, p. 37
Smith F. G., Jones D. H. P., Dick J. S. B., Pike C. D., 1988, MNRAS, 233, 305
Sparks W. B., Axon D. J., 1999, PASP, 111, 1298
Takata J., Chang H.-K., Cheng K. S., 2007, ApJ, 656, 1044
Vashakidze M. A., 1954, Astron. Circ, 147, 11
Wagner S. J., Seifert W., 2000, in Kramer M., Wex N., Wielebinski R., eds, ASP Conf. Ser., IAU Colloq. 177: Pulsar Astronomy – 2000 and Beyond, Vol. 202. Optical Polarization Measurements of Pulsars. Astron. Soc. Pac., San Francisco, p. 315
Walsh J., 1999, The ST-ECF Newsletter, Issue Number 26
Wampler E. J., Scargle J. D., Miller J. S., 1969, ApJ, 157, L1
Weisskopf M. C., Silver E. H., Kestenbaum H. L., Long K. S., Novick R., 1978, ApJ, 220, L117
Weisskopf M. C., Hester J. J., Tennant A. F., Elsnor R. F., Schulz N. S., 2000, ApJ, 536, L81
Woltjer L., 1957, Bull. Astron. Inst. Netherlands, 13, 301

This paper has been typeset from a TEX/LATEX file prepared by the author.